THE JOURNAL OF PHYSICAL CHEMISTRY C
A JOURNAL OF THE AMERICAN CHEMICAL SOCIETY

pubs.acs.org/JPCC

Article

Optimization of Eu^{3+}-to-Host Emission Ratio in Double-Perovskite Molybdenites for Highly Sensitive Temperature Sensors

Bartosz Bondzior,* Dagmara Stefańska, T. H. Q. Vu, and Przemysław J. Dereń

Cite This: *J. Phys. Chem. C* 2022, 126, 13247−13255

Read Online

ACCESS | Metrics & More | Article Recommendations | Supporting Information

ABSTRACT: Double-perovskite phosphors exhibit unusual thermal and luminescent behavior and could potentially be applied as efficient and sensitive luminescent temperature sensors. Four double perovskite hosts—Ba_2MgMoO_6 (BMM), Sr_2MgMoO_6 (SMM), Ba_2ZnMoO_6 (BZM), and Sr_2ZnMoO_6 (SZM)—are studied for the correlations between the symmetry, energetic structure, luminescence, and thermometric performance. The quantum yield of Eu^{3+} emission in those hosts is higher for the samples with high cubic symmetry and ranges up to over 20% for Ba_2MgMoO_6. The Eu^{3+} ions can be excited indirectly by the host absorption bands in the UV and charge transfer band (CTB) in the blue range. The symmetry of the host plays a crucial role in the thermal stability of the host emission, which together with varying activation energy of Eu^{3+} luminescence provides a basis for thermometric sensitivity optimization. The relative sensitivities (S_r) obtained by the Eu-doped molybdenite hosts are 3.2% at 75 °C for Sr_2MgMoO_6 and 9.2% at −196 °C for Ba_2ZnMoO_6. It is also demonstrated that the sensing performance is higher in hosts with a uniform quenching profile of host luminescence and steep quenching of Eu^{3+} luminescence.

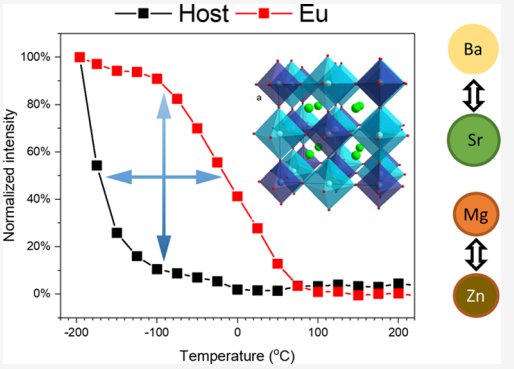

INTRODUCTION

Temperature is one of the most important physical factors that affects dynamics and viability of natural systems and is an important parameter in many physical and chemical processes. The means of performing accurate temperature measurements have an impact on scientific and human development. The technique of semicontact luminescence thermometry offers lots of advantages compared to traditional contact thermometers due to noninvasive measurement, fast response, high sensitivity, applicability in fast-evolving conditions, and strong electromagnetic fields.[1−4] Three main approaches to optical measurements of temperature are usually used: (i) spectral shift of emission band, (ii) variation of the emission intensity of a single transition or two independent transitions, and (iii) the kinetics of the emitting levels' relaxation. The first two routes are steady-state (time-integrated) techniques, while the last one is a time-resolved method. The intensity of emission depends on a couple of factors such as a material's inhomogeneity, optoelectronic drifts, excitation source, and type of detector which all may lead to inaccurate or unrepeatable measurements. Therefore, the most commonly used temperature readout is based on the relative intensity ratio of two different emission bands. This method minimizes the influence of troublesome external factors, and it is therefore called self-calibrating, dual-emitting, or ratiometric luminescence thermometry.

One of the most promising groups for semicontact temperature readout is double-perovskite materials of the general formula $A_{2-x}A_x'BB'O_6$, where A and A′ sites are occupied by alkaline metals or lanthanides, while positions B and B′ are reserved for transition-metal ions. Recently, the optical properties of many tungstate and molybdate double perovskites have been investigated, such as Ba_2MgWO_6,[5,6] Ba_2ZnWO_6,[7] Ba_2CuWO_6,[8] Sr_2CoWO_6,[9] Sr_2CaWO_6,[10] Sr_2CaMoO_6,[11] $Ca_3Mo_xW_{1-x}O_6$,[12] or Ba_2MgMoO_6.[13] Tungstate and molybdate (WO_6/MoO_6) groups can exhibit a broad emission band located in the visible region of the electromagnetic spectrum.[14−16] Usually the emission of WO_6/MoO_6 is quenched very quickly with temperature; however, for samples doped with lanthanide ions, such as Eu^{3+}, efficient energy transfer from host to dopant occurs.[17] Moreover, in these compounds, lanthanide ions can be excited through the host's strong absorption band or directly by using *f*−*f* orbitals.

The coexistence of host and rare-earth (RE) ions emission is very attractive for LEDs or thermometric applications. It has been used to obtain thermal sensitivities as high as 12.2% K^{-1} (at 300 °C) for $Zn_2SiO_4:Mn^{2+}$.[18] For the physiological temperature region (20−60 °C) the sensitivities obtained by

Received: April 27, 2022
Revised: July 18, 2022
Published: July 27, 2022

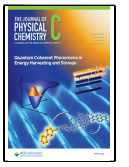

using this readout mode range from 2.6% K^{-1} for $MgTiO_3:Cr^{3+}$[19] to 10.5% K^{-1} (at 57 °C) for $TiO_2:Sm^{3+}$.[20] The Eu^{3+}-doped materials tend to generate lower thermometric sensitivities at temperature ranges unfit for physiological thermometry, e.g., 0.5% K^{-1} (at 147 °C) for $Gd_2Ti_2O_7$,[21] 2.4% K^{-1} (at 252 °C) for TiO_2,[22] and 2.2% K^{-1} (at 187 °C) for $SrZnO_3$.[23] In this paper we demonstrate the possibility to obtain high sensitivity of Eu^{3+}/host thermometry in the physiological temperature range. The thermal stability of RE luminescence can be influenced by modification of the host by host ion substitution, as demonstrated by Wang et al. in solid−solution molybdenite−tungstate double perovskites.[12]

To investigate the temperature sensing performance of molybdate double perovskites, pure and Eu^{3+}-doped hosts of Ba_2MgMoO_6 (BMM), Sr_2MgMoO_6 (SMM), Ba_2ZnMoO_6 (BZM), and Sr_2ZnMoO_6 (SZM) were prepared by the coprecipitation method. The main goal of this paper is to study the coexistence and the relation between emission of host and dopant ions. The ratio of the host-to-dopant emission intensity can be regulated by the substitution of Ba^{2+} ions with Sr^{2+} ions and of Mg^{2+} with Zn^{2+} ions. It is well-known that sample composition affects host symmetry and energy separation between MoO_6 and the charge transfer band (CTB) of Eu^{3+} levels. Therefore, the relative sensitivity (S_r) as well as useful temperature range can be tuned by changing the composition of the sample.

METHODS

Synthesis Procedures. In this study, several undoped and doped double perovskites with the chemical formula $A_2B_{1-2x}Eu_xLi_xMoO_6$ (where A = Ba^{2+}, Sr^{2+}; B = Mg^{2+}, Zn^{2+}, x = 0 and 2%) were synthesized by the coprecipitation method. Because the Eu^{3+} ions were replaced to Mg^{2+}/Zn^{2+} sites, therefore lithium ions (Li^+) were used as a charge compensator. As mentioned in a recent publication,[1] the amount of Mg^{2+} was used in excess of 20% to compensate for the sublimation of Mg^{2+} during the sintering.

The precursors including barium acetate $Ba(CH_3COO)_2$ (Alfa Aesar, 99%), strontium acetate $Sr(CH_3COO)_2{\cdot}0.5H_2O$ (Alfa Aesar, 98%), magnesium acetate $Mg(CH_3COO)_2{\cdot}4H_2O$ (Alfa Aesar, 99.95%), zinc acetate $Zn(CH_3COO)_2{\cdot}2H_2O$ (POCH, 99.5%), ammonium molybdate $(NH_4)_6Mo_7O_{24}{\cdot}4H_2O$ (Thermal Scientific Acros, >99%), europium acetate $Eu(CH_3COO)_3$ (Alfa Aesar, 99.9%), and lithium carbonate Li_2CO_3 (Alfa Aesar, 99%) were used without further purification.

First, the stoichiometric amounts of precursors calculated for 0.5 g of final product were weighed and dissolved separately in a proper amount of distilled water to produce clear solutions under a constant stirring speed of 200 rpm. Second, the solutions of molybdate, Ba^{2+}/Sr^{2+}, Mg^{2+}/Zn^{2+}, and Eu^{3+} were gently mixed to form a precipitate. The obtained precipitate was dried at 80 °C on a hot plate overnight. Third, the precipitate was ground in an agate mortar for 10 min. After that, the fine powder was sintered at 600 °C for 12 h in a furnace in air. The second sintering temperature was optimized for each sample. It was found to be at 1150 °C for BMM, 1050 °C for BZM, 1200 °C for SMM, and 1000 °C for SZM. The second sintering time was 6 h.

Characterization. The crystal structure was studied by using an X'Pert ProPANalytical X-ray diffractometer (PANalytical, Almelo, The Netherlands) with Cu Kα radiation (λ = 1.54056 Å) for 2θ ranging from 10° to 90°. Emission spectra were recorded by a Hamamatsu R928 photomultiplier (Hamamatsu Photonics K.K, Shizuoka, Japan) with a Nd:YAG-pumped Ti:sapphire laser as an excitation source. Excitation spectra were measured by using a McPherson spectrometer with a 150 W xenon lamp. Emission kinetic profiles were recorded by a Lecroy digital oscilloscope (Teledyne LeCroy, New York, NY) with a Nd:YAG-pumped Ti:sapphire laser as the excitation source. The temperature of the sample was controlled by a Linkam THMS 600 heating/freezing stage (The McCRONE Group, Westmont, IL).

RESULTS AND DISCUSSION

Structural Properties. There is no standard pattern for BMM and BZM; however, it matches well the ICSD pattern of Ba_2MgWO_6 (see Figure 1a), which is also confirmed by Zhang

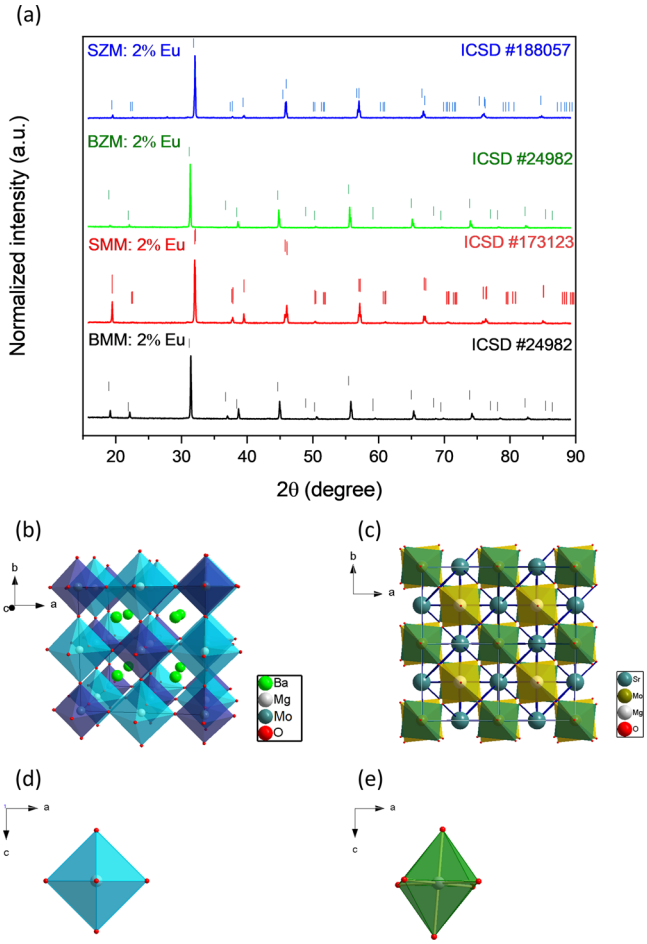

Figure 1. (a) XRD results of the studied hosts doped with 2% Eu^{3+} with relevant ICSD patterns. (b) Unit cell of BMM with the space group $Fm\bar{3}m$. (c) Unit cell of SMM with the space group $I1$. (d) Mg/Zn−O octahedra in the space group $Fm\bar{3}m$. (e) Mg/Zn−O octahedra in the space group $I1$.

et al.[24] In the case of SMM and SZM,[25] it was found that both crystallized in a lower symmetry than BMM and BZM, namely, $I1$-(2) triclinic and $I4/m$ (87) tetragonal, respectively (see Figure 1a). The BMM and BZM are therefore assumed to have a perfect double-perovskite structure represented in Figure 1b, while the SMM and SZM hosts exhibit deviations from the perfect cubic symmetry as depicted in Figure 1c. BMM and BZM possess an ideal Mg(Zn)−O octahedra with six equal

https://doi.org/10.1021/acs.jpcc.2c02924
J. Phys. Chem. C 2022, 126, 13247−13255

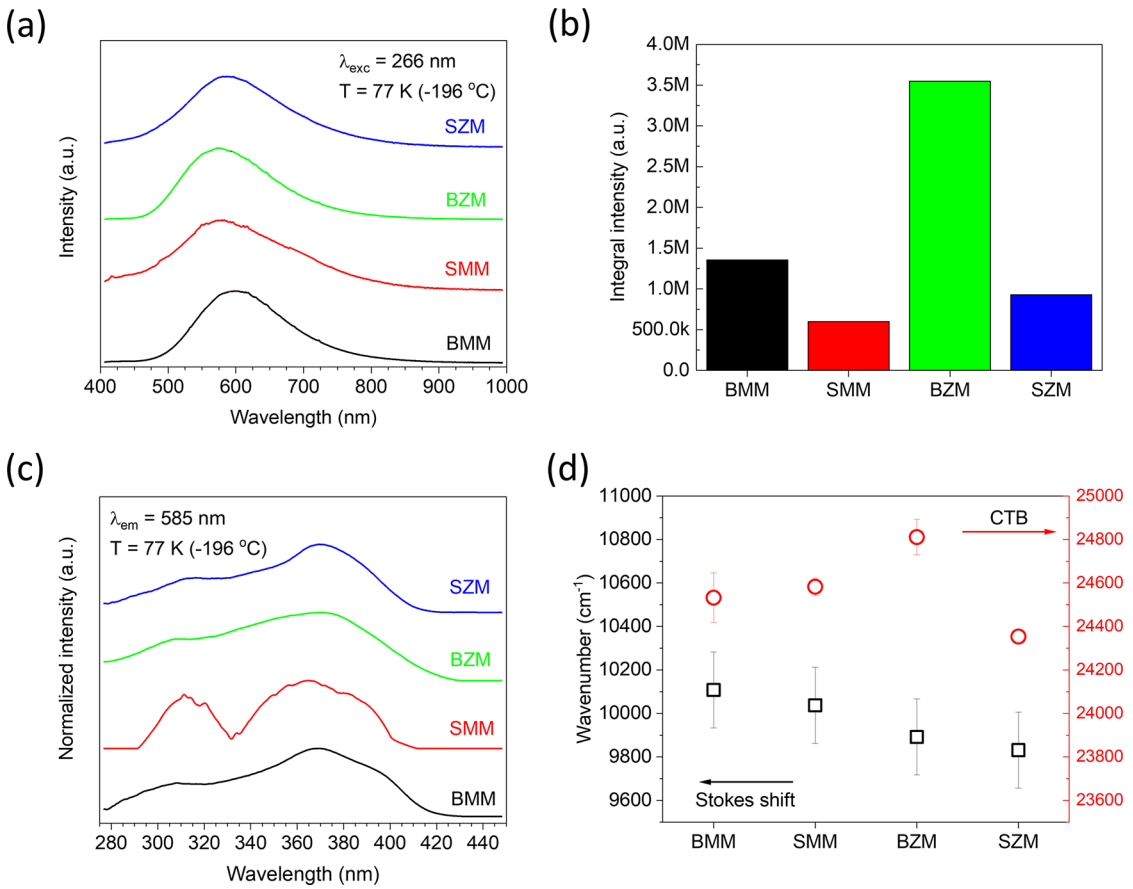

Figure 2. (a) Emission spectra of the double-perovskite hosts, (b) intensity of the host luminescence, (c) PLE spectra of undoped host materials, and (d) Stokes shift of host emission and charge transfer band energy for Eu^{3+} PLE.

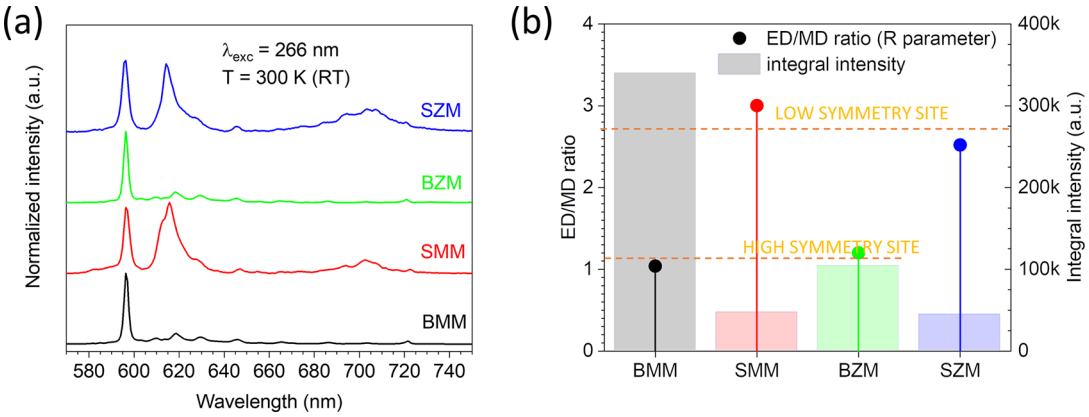

Figure 3. (a) Emission spectra of Eu^{3+}-doped double perovskites. (b) Luminescence intensity of Eu^{3+} (bars) and the ED/MD ratio (circles) of Eu^{3+}.

bonds of 2.1902 Å, three angles of 180°, and 12 angles of 90° (Figure 1b,d). As can be seen in Figure 1c,e, in the triclinic SMM structure the octahedral moiety is tilted due to the distortion of Mg(Zn)−O interatomic distances and O−Mg(Zn)−O bond angles deviating from the ideal angles of 180° and 90° by about 0.014° and 5.322°, respectively. The above findings were also confirmed by the tolerance factor (t)[26] which was calculated as 1.03 for BMM and BZM and as 0.97 for SMM and SZM. The distances between the ions are based on the available crystallographic data. According to them, the shortest Mg/Zn^{2+}−O^{2-} distance decreases when Sr^{2+} substitutes Ba^{2+} (from 2.19 to ∼2.02 Å for BMM and SMM), but the Mo^{6+}−O^{2-} shortest distance increases (from 1.87 to 1.93 Å, as above). The substitution of Zn^{2+} for Mg^{2+} should have a small impact on the structure and distances because their relative ionic radii difference is 2% compared to 11% for Ba^{2+} and Sr^{2+}. The substitutions of Sr^{2+} for Ba^{2+} in BZM and SZM are expected to have a smaller impact on the ionic distances because the difference in unit cell volume between BZM and SZM is much smaller (534.6 to 521 Å) than in BMM and SMM (533.4 to 491.6 Å).

Luminescence. All the studied hosts exhibit similar broad band emission in the orange-red region (500−800 nm), as seen in Figure 2a. The emission results from the Mo−O charge

https://doi.org/10.1021/acs.jpcc.2c02924
J. Phys. Chem. C 2022, 126, 13247−13255

transfer (CT) transition, which was previously implied by Zhang et al.,[24] but not observed at room temperature due to strong thermal quenching. Such host luminescence was observed in molybdenites by Wiegel and Blasse,[27] and the spectral characteristic they observed for Ba_2CaMoO_6 and Sr_2CaMoO_6 resembles our results. The BZM host displays the most intense luminescence, and the sample containing Sr displays a weaker luminescence compared to their Ba-containing analogues (see Figure 2b).

The photoluminescence excitation (PLE) spectra of the undoped hosts exhibit little to no variation among the samples (see Figure 2c). Similarly to tungstate double perovskites, the PLE spectra can be decomposed into two components: one with a lower wavenumber resulting from the $O^{2-} \rightarrow Mo^{6+}$ CT and a one with a higher wavenumber associated with the excitation of the Ba/Sr states in the conduction band.[16] The resulting values of the Stokes shift calculated as a difference of energy between the lower excitation band and the emission band (see Figure 2d) are typical for MoO_6 groups[27] and decrease in the order BMM > SMM > BZM > SZM.

The emission spectra of Eu-doped double-perovskite molybdenites uncover a fundamental difference in the luminescence properties of samples containing Ba^{2+} and Sr^{2+}. The former exhibit strong Eu^{3+} luminescence (see Figure 3a) characteristic for high-symmetry octahedral site O_h, with dominant magnetic-dipole type $^5D_0 \rightarrow {}^7F_1$ transition at 597 nm. The latter exhibit more common Eu^{3+} luminescence characteristic for a lower symmetry site with a dominant electric dipole type $^5D_0 \rightarrow {}^7F_2$ transition at 618 nm. These results can be used to calculate the ED/MD ratio (see Figure 3b) and correlate with the calculated tolerance factors in the previous section.

The PLE spectra of Eu^{3+}-doped double-perovskite molybdenites are almost identical with ones measured for undoped hosts, with an additional low-wavenumber component resulting from the $O^{2-} \rightarrow Eu^{3+}$ charge transfer transition located in the 400−450 nm region (see Figure S1). The direct comparison to undoped samples helps to separate it from the higher energy $O^{2-} \rightarrow Mo^{6+}$ CT. The $O^{2-} \rightarrow Eu^{3+}$ CT energy is the highest for BZM and the lowest for SZM (see Figure 2d), which results from decreasing Eu−O distance[28] indicated by the structural results, given that the Eu^{3+} ions are located at Mg/Zn^{2+} site. No lines originating the Eu^{3+} *4f*−*4f* transitions were observed on the PLE spectra.

The quantum yield of the Eu^{3+} luminescence is substantially higher for highly symmetrical samples BMM and BZM (see Table 1). This is a result of an efficient energy transfer from

Table 1. Quantum Yield of Eu^{3+} Luminescence

sample	QY Eu^{3+} (±5%) (λ_{exc} = 370 nm)
BMM	20.6
SMM	1.2
BZM	5.6
SZM	2.3

the MoO_6 groups (see Figure S2) in highly symmetrical double perovskites as previously reasoned for similar tungstate hosts.[16]

Energetic Structure. The energy values of excitation and emission of undoped hosts and Eu^{3+}-doped samples allow to construct a simple diagram of the material's energetic structure (see Figure 4.) The Ba/Sr states are located in the CB and constituted by the 5d electron states of Ba/Sr^{2+} host ions as

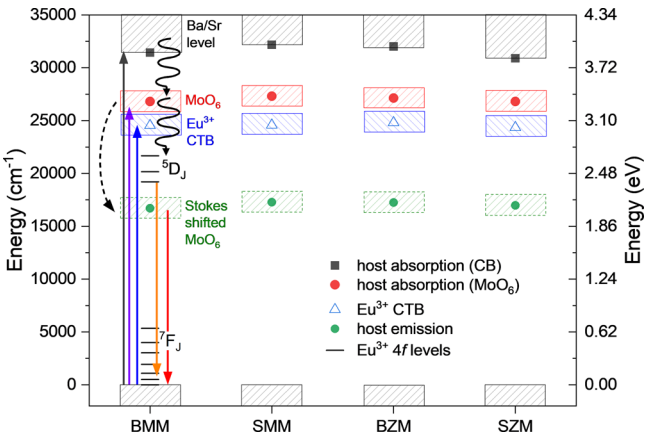

Figure 4. Energy diagram of the studied materials: black, purple, and blue solid arrows signify excitation transitions; orange and red solid arrows signify emission of Eu^{3+} and MoO_6 groups, respectively; wavy arrows signify nonradiative transitions; and the dashed arrow illustrates the Stokes shift of MoO_6 luminescence.

opposed to the 4d electron states of Mo^{6+}.[29] The position of the former is determined by the upper component of the host excitation spectrum, analogically to the double-perovskite tungstates.[16] Several simplifications need to be done as long as they are irrelevant to the quantitative outcome; for example, the $^7F_0$ level of Eu^{3+} is assumed to be located at 0 for all matrices, just to illustrate the thermal relaxation and the radiative transitions in Eu^{3+}. The MoO_6 group levels, the Eu^{2+} ground state (Eu^{3+} CTB), and the Ba/Sr levels of the conduction band are depicted with actual values relative to the valence band but disregarding the Stokes shift (illustrated by energy band of MoO_6 group shifted downward).

When Ba^{2+} ions in BMM are substituted with Sr^{2+}, all the energy levels shift upward, as typical for type I material according to Dorenbos (where going from Ba via Sr to Ca the conduction band tends to shift toward higher energies),[30] and the separation between the Eu^{3+} CTB and the MoO_6 group level grows. Substitution of the Zn^{2+} for Mg^{2+} in BMM yields virtually no consequence on the energy levels; however, the substitution of Sr^{2+} for Ba^{2+} in BZM shifts the Ba/Sr energy levels downward as well as increases the Eu^{3+} CTB−MoO_6 group levels separation. No upward shift was observed, probably due to aforementioned small difference in the unit cell volume—a much less significant contraction of the structure as a result of Sr^{2+} substitution.

The bandgap energy can also be calculated from the chemical compositions and atomic densities of the hosts materials.[31] The obtained values are higher than those observed in the excitation spectra (see Table 2).

Temperature Sensing. In all samples the host emission gets quenched at lower temperature than the Eu^{3+} emission (see Figure 5a−d). This property is the key for utilizing the FIR method for temperature sensing. The stable emission of

Table 2. Calculated Bandgap Values of Studied Hosts[31]

sample	bandgap (eV)
BMM	4.1
SMM	4.9
BZM	4.7
SZM	4.5

https://doi.org/10.1021/acs.jpcc.2c02924
J. Phys. Chem. C 2022, 126, 13247−13255

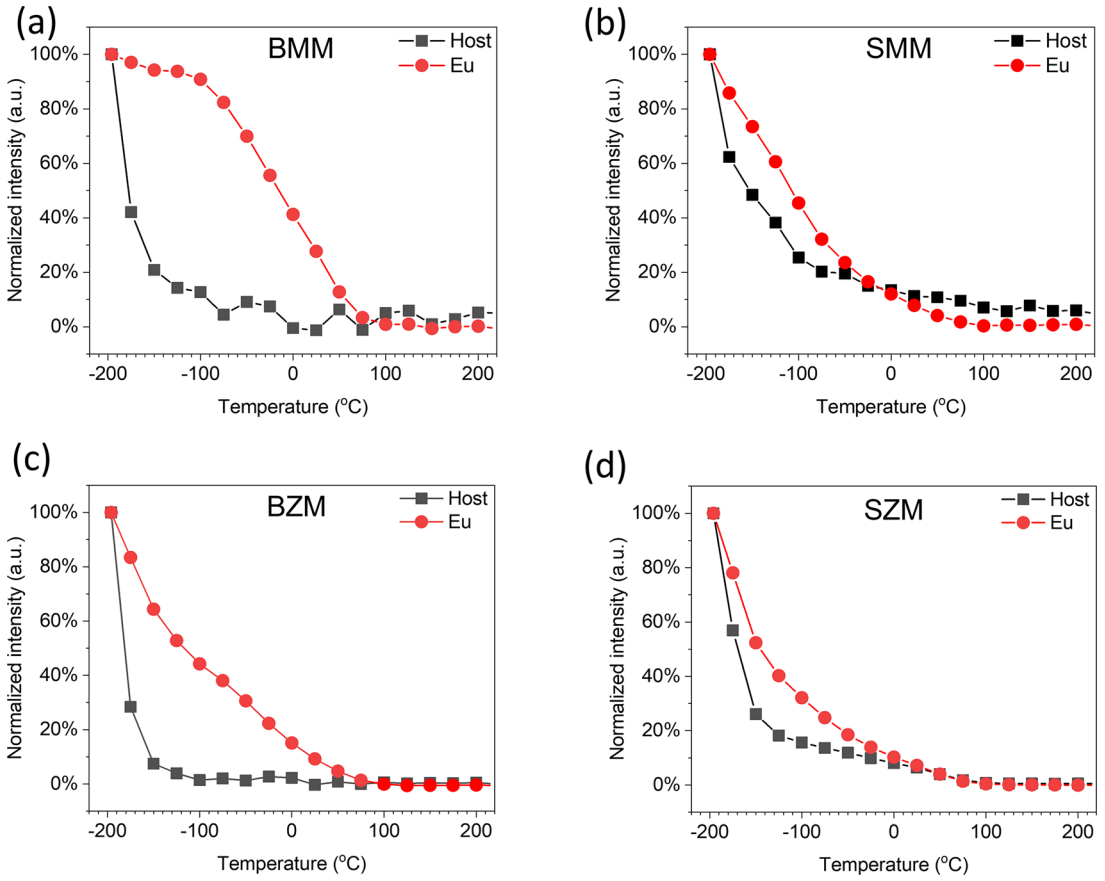

Figure 5. Thermal dependence of host and Eu^{3+} emission intensity in BMM (a), SMM (b), BZM (c), and SZM (d).

one emission center accompanied by the temperature sensitive emission of another center constitutes high thermal sensitivity of the luminescent material.

The shape of the thermal quenching curve indicates the number of quenching components and respective activation energies (fitted with luminescence thermal quenching equation;[30] see Figure S3). In the case of BMM and BZM host luminescence, the quenching curves are single components, and the activation energies are fitted to be equal to 219 and 365 cm^{-1}, respectively (see Figure 6a). Such a small value may arise from the substantial Stokes shift, as indicated on the exaggerated single coordinate diagram (Figure S4), and the larger activation energy of the Zn-based host compared to the Mg-based one might result from the slightly smaller Stokes shift (see Figure 2d). The thermal quenching curves of the SMM and SZM host luminescence exhibit two components and corresponding two separate activation energies (ΔE_1 host and ΔE_2 host) as a result of nonequivalent positions of Mo^{6+} in the lower symmetry structure, as indicated by the structural studies. Similar to BMM and BZM, these values are higher for Zn-containing hosts, also due to a lower Stokes shift.

The Eu^{3+} luminescence has two thermal quenching components for all samples (see Figure 6a). The smaller activation energies (ΔE_1 Eu^{3+}) are the same for all samples within the measurement error range. The larger activation energies (ΔE_2 Eu^{3+}) can be correlated to the separation between the CTB and the MoO_6 group energy level (see Figure 4), which indicates the thermalization of Eu^{3+} back into the MoO_6 groups.

The FIR was calculated as a ratio of Eu^{3+} to host luminescence (eq 1).

$$\mathrm{FIR}(T) = \frac{I_{Eu^{3+}}(T)}{I_{host}(T)} \tag{1}$$

The relative sensitivity S_r was derived from eq 2.

$$S_r(T) = \frac{1}{\mathrm{FIR}(T)}\frac{\mathrm{dFIR}(T)}{\mathrm{d}T} \tag{2}$$

The resulting sensitivity (S_r) for all samples (see Figure 6b) allows to identify the deciding properties of highly sensitive luminescent thermometer-based Eu^{3+}-to-host luminescence ratio. The highest S_r at low temperatures was observed for BMM and BZM (6.2% and 9.2% K^{-1} at −196 °C, respectively) due to the uniform thermal quenching profile of the host luminescence with low activation energy. SMM and SZM, due to two components of quenching, have a less steep quenching profile which amounted to 1.3 and 1.8% K^{-1} at −196 °C, respectively. At temperatures close to room temperature the deciding factor, beside the mere presence of both host and Eu^{3+} emission, was the steepness and uniformity of the Eu^{3+} quenching profile. BMM and BZM have the lowest difference of their Eu^{3+} activation energies and exhibit the steepest quenching curve; however, their host emission is totally quenched at this temperature. SMM exhibits a relatively steep Eu^{3+} quenching profile, which amounts to S_r equal to 3.2% K^{-1} at 75 °C. SZM with the largest activation energy difference has S_r equal 1.3% K^{-1} at the same temperature.

The thermal resolution δT (see Figure 6c) was determined from eq 3

https://doi.org/10.1021/acs.jpcc.2c02924
J. Phys. Chem. C 2022, 126, 13247−13255

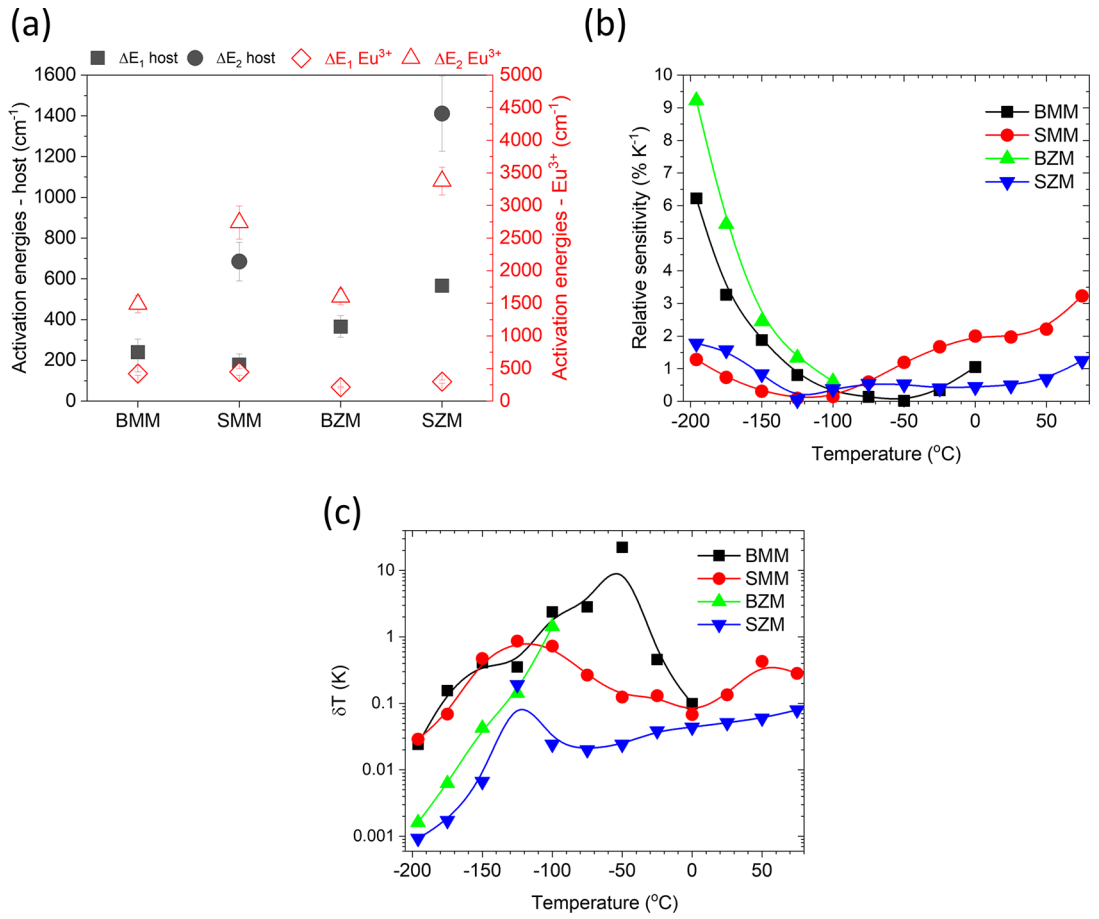

Figure 6. (a) Activation energies of thermal quenching, (b) relative thermometric sensitivities, and (c) thermal resolutions.

$$\delta T = \frac{1}{S_r}\frac{\delta \mathrm{FIR}}{\mathrm{FIR}} \tag{3}$$

where δFIR is calculated based on the measurement uncertainties of the host and Eu emission intensity. The minimum of thermal resolution for all samples is for the lowest temperature. The thermal resolution goes below 0.01 K only for BZM and SZM for temperatures below −175 and −150 °C, respectively. BMM and SMM have a poor thermal resolution of 0.01−1 K in the usable range. In the higher temperature—close to the room temperature—range SZM, despite having lower sensitivity, has thermal resolution below 0.1 K compared to 0.2−0.4 K for SMM. This superiority of Zn-based materials in terms of thermal resolution indicates that the intensity of the host luminescence (see Figure 2b) is the determining factor, as opposed to Eu^{3+} luminescence (see Figure 3b).

Decay Times. The host luminescence exhibits a multi-exponential decay curve after an impulse excitation at 370 nm (see Figure 7a). To compare the decay curves quantitatively, the mean decay time was calculated as eq 4 (see Figure 7b):

$$\tau_{\mathrm{host}} = \frac{\int tI(t)\,\mathrm{d}t}{\int I(t)\,\mathrm{d}t} \tag{4}$$

The mean decay times follow a reverse trend to thermal quenching activation energy of the host luminescence. The decay times of the Ba-based hosts are longer than those of Sr-based hosts, which indicates the impact of symmetry on the lifetime of the MoO_6 group excited level. Also, the decay times of Zn-based hosts are slightly longer than those of the corresponding Mg-based analogues. This may result from the higher activation energies for nonradiative depopulation of excited states (see Figure 6a).

The decay curves of Eu^{3+} luminescence have two to three distinct components: one/two in the 100 μs−5 ms range, typical for Eu^{3+} luminescence lifetime (one for BMM and BZM; two for SMM and SZM), and much longer decay component in tens of milliseconds indicative of the processes involving defects and persistent luminescence (see Figure 7c). The shortest decay components observed for SMM and SZM, in hundreds of microseconds, are denoted as τ_1 (see Figure 7d), the millisecond components are denoted as τ_2 (see Figure 7e), and the longest components are denoted as τ_3 (Figure 7f).

The τ_2 (see Figure 7e) follows a similar trend as host emission decay, which is consistent with higher symmetry of the Ba-based hosts. The decay time for SZM, however, is longer than that of BMM, which indicates that Zn-based hosts provide a more stable excited state of Eu^{3+}, which seem to contradict the fact that Zn-based hosts exhibit lower activation energies of Eu^{3+}.

The additional τ_1 components of Eu^{3+} luminescence decay in SMM and SZM result from lower symmetry and two inequivalent crystallographic sites for Mg/Zn, in which the Eu^{3+} ions enter. The short component is longer for SZM, similarly to τ_2.

The τ_1 and τ_2 of decay curves measured at room temperature are longer than at low temperature, and the longest component is not recorded at all. This confirms the

https://doi.org/10.1021/acs.jpcc.2c02924
J. Phys. Chem. C 2022, 126, 13247−13255

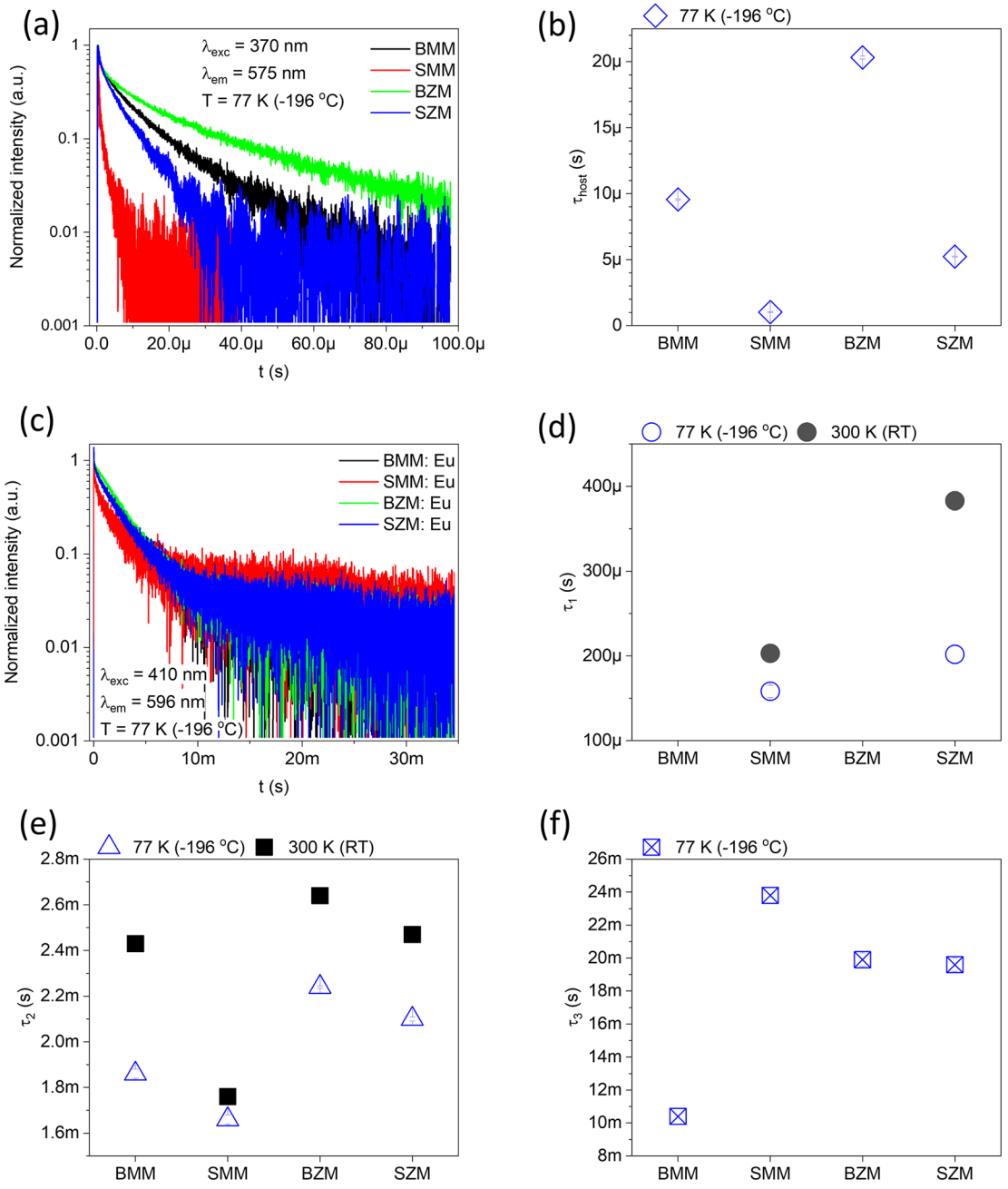

Figure 7. (a) Luminescence decay curves of host emission, (b) mean decay time values of host emission, (c) luminescence decay curves of Eu^{3+} emission, and (d–f) decay constants of decay components.

origin of the persistent luminescence from defect states, which at room temperature efficiently feed the excited states of Eu^{3+}.[32]

The long decay component of Eu^{3+} luminescence (see Figure 7f) is the longest for SMM with decay time equal 24 ms and the shortest for BMM with 10 ms. This luminescence is most likely to originate from the trapping states (defect states or other energy levels) within the bandgap, and the decay time is directly linked to their separation from the CB states. That hypothesis is supported by the fact that the BMM and SMM have respectively the lowest and the highest bandgap energy (see Table 2). The presence of defects in studied hosts results from the fact that trivalent Eu dopant enters a divalent Mg/Zn site, causing a charge imbalance, which is generally compensated by monovalent Li dopant but nonetheless can introduce local structural impurities.

CONCLUSIONS

Four double-perovskite hosts doped with Eu^{3+} ions exhibit luminescence originating from both MoO_6 group charge transfer transition (orange red) and standard Eu^{3+} luminescence. The substitution of Ba ions with Sr and Mg ions with Zn has an impact on the symmetry of the host—in accordance with the tolerance factor determined from the ionic radii—and, in consequence, affects the luminescent properties.

The host luminescence at 77 K is the most intense for the BZM sample, and the Eu^{3+} luminescence has the highest quantum yield for samples with cubic symmetry: BMM and BZM − 20.6% and 5.6%, respectively. The Eu^{3+} luminescence

https://doi.org/10.1021/acs.jpcc.2c02924
J. Phys. Chem. C 2022, 126, 13247−13255

has long-living components—up to 24 ms for SMM—due to the structural defect states.

The highest relative sensitivity of FIR luminescence thermometry is achieved for BZM (9.2% K^{-1} at −196 °C) and SMM (3.2% K^{-1} at 75 °C). From the comparison between hosts and the analysis of thermal quenching components, the factors responsible for high thermometric sensitivity are identified as the uniform quenching profile of host luminescence and steep quenching of Eu^{3+} luminescence.

This work will allow for further systematic studies on other double-perovskite hosts for the rare earth luminescent dopants in the context of luminescent thermometry and other applications. BMM and BZM hosts are promising hosts for high QY emitters.

■ ASSOCIATED CONTENT

Supporting Information

The Supporting Information is available free of charge at https://pubs.acs.org/doi/10.1021/acs.jpcc.2c02924.

PLE spectra host and Eu-doped samples; fitting curves of thermal quenching of samples luminescence; exaggerated single coordinate diagram of interdependence of the Stokes shift and activation energy of nonradiative relaxation (PDF)

■ AUTHOR INFORMATION

Corresponding Author

Bartosz Bondzior − *Institute of Low Temperature and Structure Research, Polish Academy of Sciences, 50-422 Wrocław, Poland; Laboratory of Photonics, Tampere University, 33720 Tampere, Finland;* orcid.org/0000-0002-1764-2427; Email: b.bondzior@intibs.pl

Authors

Dagmara Stefańska − *Institute of Low Temperature and Structure Research, Polish Academy of Sciences, 50-422 Wrocław, Poland;* orcid.org/0000-0002-1051-3761

T. H. Q. Vu − *Institute of Low Temperature and Structure Research, Polish Academy of Sciences, 50-422 Wrocław, Poland;* orcid.org/0000-0001-9390-3994

Przemysław J. Dereń − *Institute of Low Temperature and Structure Research, Polish Academy of Sciences, 50-422 Wrocław, Poland;* orcid.org/0000-0001-6316-6954

Complete contact information is available at: https://pubs.acs.org/10.1021/acs.jpcc.2c02924

Author Contributions

The manuscript was written through contributions of all authors. All authors have given approval to the final version of the manuscript. B.B.: conceptualization, data curation, formal analysis, investigation, methodology, writing of original draft, visualization; D.S.: conceptualization, data curation, formal analysis, investigation, methodology, writing of original draft, writing, review, and editing; T.H.Q.V.: conceptualization, data curation, formal analysis, investigation, methodology, writing of original draft, writing, review, and editing, validation, visualization; P.J.D.: conceptualization, funding acquisition, methodology, project administration, supervision, writing, review, and editing.

Notes

The authors declare no competing financial interest.

■ ACKNOWLEDGMENTS

The authors thank E. Bukowska, M.SC., for the XRD measurements. This work was supported by the Polish National Science Centre under Grant 2017/25/B/ST5/02670 as part of the research project OPUS13.

■ REFERENCES

(1) Li, B.; Wen, H. M.; Cui, Y.; Qian, G.; Chen, B. Multifunctional Lanthanide Coordination Polymers. *Prog. Polym. Sci.* **2015**, *48*, 40−84.

(2) Zhao, D.; Cui, Y.; Yang, Y.; Qian, G. Sensing-Functional Luminescent Metal-Organic Frameworks. *CrystEngComm* **2016**, *18* (21), 3746−3759.

(3) Hu, Z.; Deibert, B. J.; Li, J. Luminescent Metal−Organic Frameworks for Chemical Sensing and Explosive Detection. *Chem. Soc. Rev.* **2014**, *43* (16), 5815−5840.

(4) Cui, Y.; Zhang, J.; He, H.; Qian, G. Photonic Functional Metal−Organic Frameworks. *Chem. Soc. Rev.* **2018**, *47* (15), 5740−5785.

(5) Vu, T. H. Q.; Bondzior, B.; Stefańska, D.; Miniajluk, N.; Dereń, P. J. Synthesis, Structure, Morphology, and Luminescent Properties of Ba_2MgWO_6: Eu^{3+} Double Perovskite Obtained by a Novel Co-Precipitation Method. *Materials (Basel)* **2020**, *13* (7), 1614.

(6) Stefańska, D.; Bondzior, B.; Vu, T. H. Q.; Miniajluk-Gaweł, N.; Dereń, P. J. The Influence of Morphology and Eu^{3+} Concentration on Luminescence and Temperature Sensing Behavior of Ba_2MgWO_6 Double Perovskite as a Potential Optical Thermometer. *J. Alloys Compd.* **2020**, *842*, 155742.

(7) Chen, P.; Yang, D.; Hu, W.; Zhang, J.; Wu, Y. Photoluminescence Properties and Structure of Double Perovskite Ba_2ZnWO_6:Eu^{3+}, Li^+ as a Novel Red Emitting Phosphor. *Chem. Phys. Lett.* **2017**, *689*, 169−173.

(8) Reinen, D.; Weitzel, H. Die Kristallstrukturen Cu^{2+}-Haltiger Oxidischer Elpasolithe - Neutronenbeugungsuntersuchungen an Den Kristallpulvern. *Zeitschrift fur Anorg. und Allg. Chemie* **1976**, *424* (1), 31−38.

(9) Viola, M. C.; Martínez-Lope, M. J.; Alonso, J. A.; Martínez, J. L.; De Paoli, J. M.; Pagola, S.; Pedregosa, J. C.; Fernández-Díaz, M. T.; Carbonio, R. E. Structure and Magnetic Properties of Sr_2CoWO_6 : An Ordered Double Perovskite Containing Co^{2+} (HS) with Unquenched Orbital Magnetic Moment. *Chem. Mater.* **2003**, *15* (8), 1655−1663.

(10) Gateshki, M.; Igartua, J. M. Crystal Structures and Phase Transitions of the Double-Perovskite Oxides Sr_2CaWO_6 and Sr_2MgWO_6. *J. Phys.: Condens. Matter* **2004**, *16* (37), 6639−6649.

(11) Ye, S.; Yu, D. C.; Wang, X. M.; Song, E. H.; Zhang, Q. Y. Anomalous Upconversion Emission of Eu^{3+}−Yb^{3+}−MoO_6 in Double Perovskites Induced by a Laser. *J. Mater. Chem. C* **2013**, *1* (8), 1588−1594.

(12) Wang, C.; Ye, S.; Li, Y.; Zhang, Q. The Impact of Local Structure Variation on Thermal Quenching of Luminescence in $Ca_3Mo_xW_{1-x}O_6$:Eu^{3+} Solid Solution Phosphors. *J. Appl. Phys.* **2017**, *121* (12), 123105.

(13) Zhang, L.; Sun, B.; Shao, C.; Zhen, F.; Wei, S.; Bu, W.; Yao, Q.; Jiang, Z.; Chen, H. Preparation, Band-Structure and Luminescence of Double Perovskite Ba_2MgMoO_6:Eu^{3+} Orange-Red Phosphor for White LEDs. *Ceram. Int.* **2018**, *44* (14), 17305−17312.

(14) Bode, J. H. G.; Van Oosterhout, A. B. Defect Luminescence of Ordered Perovskites A_2BWO_6. *J. Lumin.* **1975**, *10* (4), 237−242.

(15) Blasse, G.; Corsmit, A. F. Electronic and Vibrational Spectra of Ordered Perovskites. *J. Solid State Chem.* **1973**, *6* (4), 513−518.

(16) Bondzior, B.; Vu, T. H. Q.; Stefańska, D.; Winiarski, M. J.; Dereń, P. J. Tunable Broadband Emission by Bandgap Engineering in $(Ba,Sr)_2(Mg,Zn)WO_6$ Inorganic Double-Perovskites. *J. Alloys Compd.* **2021**, *888*, 161567.

(17) Vu, Q. T. H.; Bondzior, B.; Stefańska, D.; Miniajluk-Gaweł, N.; Winiarski, M. J.; Dereń, P. J. On How the Mechanochemical and Co-Precipitation Synthesis Method Changes the Sensitivity and Operating Range of the $Ba_2Mg_{1-x}Eu_xWO_6$ Optical Thermometer. *Sci. Rep.* **2021**, *11* (1), 22847.

(18) Lojpur, V.; Nikolić, M. G.; Jovanović, D.; Medić, M.; Antić, Ž.; Dramićanin, M. D. Luminescence Thermometry with Zn_2SiO_4:Mn^{2+} Powder. *Appl. Phys. Lett.* **2013**, *103* (14), 141912.
(19) Ćirić, A.; Periša, J.; Medić, M.; Kuzman, S.; Ristić, Z.; Antić, Ž.; Dramićanin, M. D. Sensitive Temperature Reading from Intensity Ratio of Cr^{3+} and Defects' Emissions in $MgTiO_3$:Cr^{3+}. *Ceram. Int.* **2021**, *47* (22), 31915−31919.
(20) Dramićanin, M. D.; Antić; Ćulubrk, S.; Ahrenkiel, S. P.; Nedeljković, J. M. Self-Referenced Luminescence Thermometry with Sm^{3+} Doped TiO_2 Nanoparticles. *Nanotechnology* **2014**, *25* (48), 485−501.
(21) Lojpur, V.; Ćulubrk, S.; Dramićanin, M. D. Ratiometric Luminescence Thermometry with Different Combinations of Emissions from Eu^{3+} Doped $Gd_2Ti_2O_7$ Nanoparticles. *J. Lumin.* **2016**, *169*, 534−538.
(22) Nikolić, M. G.; Antić, Ž.; Ćulubrk, S.; Nedeljković, J. M.; Dramićanin, M. D. Temperature Sensing with Eu^{3+} Doped TiO_2 Nanoparticles. *Sensors Actuators, B Chem.* **2014**, *201*, 46−50.
(23) Das, S.; Som, S.; Yang, C. Y.; Chavhan, S.; Lu, C. H. Structural Evaluations and Temperature Dependent Photoluminescence Characterizations of Eu^{3+}-Activated $SrZrO_3$ Hollow Spheres for Luminescence Thermometry Applications. *Sci. Rep.* **2016**, *6* (1), 1−13.
(24) Zhang, S.; Hu, Y.; Chen, L.; Wang, X.; Ju, G.; Fan, Y. A Novel Ba_2MgMoO_6 :Eu^{3+} Orange-Red Phosphor: Photoluminescence Properties and Mechanism of Charge and Energy Transfer. *J. Mater. Res.* **2013**, *28* (22), 3130−3136.
(25) Filonova, E. A.; Dmitriev, A. S. Crystal Structure and Thermal Properties of Sr_2ZnMoO_6. *Inorg. Mater.* **2013**, *49* (6), 602−605.
(26) Hossain, A.; Bandyopadhyay, P.; Roy, S. An Overview of Double Perovskites $A_2B'B''O_6$ with Small Ions at A Site: Synthesis, Structure and Magnetic Properties. *J. Alloys Compd.* **2018**, *740*, 414−427.
(27) Wiegel, M.; Blasse, G. The Luminescence Properties of Octahedral and Tetrahedral Molybdate Complexes. *J. Solid State Chem.* **1992**, *99* (2), 388−394.
(28) Blasse, G. On the Eu3+ Fluorescence of Mixed Metal Oxides. IV. The Photoluminescent Efficiency of Eu^{3+} -Activated Oxides. *J. Chem. Phys.* **1966**, *45* (7), 2356−2360.
(29) Winiarski, M. J.; Dereń, P. Electronic Structure of AB'B''O_6-Type (A = Ca, Sr, Ba; B' = Mg, Zn; B'' = Mo, W) Double Perovskite Oxides. *Opt. Mater. (Amst).* **2019**, *90*, 95−98.
(30) Dorenbos, P. Thermal Quenching of Eu^{2+} 5d−4f Luminescence in Inorganic Compounds. *J. Phys.: Condens. Matter* **2005**, *17* (50), 8103−8111.
(31) Korotkov, A. S.; Atuchin, V. V. Prediction of Refractive Index of Inorganic Compound by Chemical Formula. *Opt. Commun.* **2008**, *281* (8), 2132−2138.
(32) Michalik, D.; Pawlik, T.; Kukliński, B.; Lazarowska, A.; Leśniewski, T.; Barzowska, J.; Mahlik, S.; Grinberg, M.; Adamczyk, B.; Pławecki.; et al. Dopant Concentration Induced Optical Changes in Ca,Eu-α-Sialon. *Crystals* **2017**, *7* (11), 342.

https://doi.org/10.1021/acs.jpcc.2c02924
J. Phys. Chem. C 2022, 126, 13247−13255